NANO LETTERS

Letter

Cite This: Nano Lett. 2018, 18, 7524−7528

pubs.acs.org/NanoLett

Guided by Light: Optical Control of Microtubule Gliding Assays

Roderick P. Tas,[†,⊥] Chiung-Yi Chen,[†,⊥] Eugene A. Katrukha,[†] Mathijs Vleugel,[§] Maurits Kok,[§] Marileen Dogterom,[§] Anna Akhmanova,[†] and Lukas C. Kapitein*[,†]

[†]Department of Biology, Faculty of Science, Utrecht University, 3584 CH Utrecht, The Netherlands

[§]Department of Bionanoscience, Kavli Institute of Nanoscience, Delft University of Technology, van der Maasweg 9, 2629 HZ Delft, The Netherlands

Supporting Information

ABSTRACT: Force generation by molecular motors drives biological processes such as asymmetric cell division and cell migration. Microtubule gliding assays in which surface-immobilized motor proteins drive microtubule propulsion are widely used to study basic motor properties as well as the collective behavior of active self-organized systems. Additionally, these assays can be employed for nanotechnological applications such as analyte detection, biocomputation, and mechanical sensing. While such assays allow tight control over the experimental conditions, spatiotemporal control of force generation has remained underdeveloped. Here we use light-inducible protein−protein interactions to recruit molecular motors to the surface to control microtubule gliding activity in vitro. We show that using these light-inducible interactions, proteins can be recruited to the surface in patterns, reaching a ∼5-fold enrichment within 6 s upon illumination. Subsequently, proteins are released with a half-life of 13 s when the illumination is stopped. We furthermore demonstrate that light-controlled kinesin recruitment results in reversible activation of microtubule gliding along the surface, enabling efficient control over local microtubule motility. Our approach to locally control force generation offers a way to study the effects of nonuniform pulling forces on different microtubule arrays and also provides novel strategies for local control in nanotechnological applications.

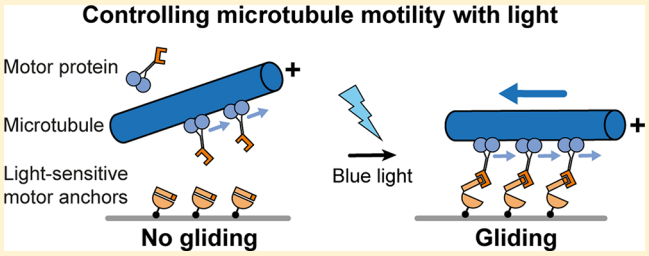

KEYWORDS: *Microtubules, motor proteins, optical control, optogenetics*

Force generation by molecular motors on the microtubule cytoskeleton drives biological processes such as asymmetric cell division and cell migration. To better understand these processes, in vitro reconstitution assays are often used to decipher the underlying interactions and principles.[1−3] Microtubule gliding assays in which motor proteins are immobilized on the surface to propel microtubules, are a widely used example of such experiments. Applications of these assays range from studying basic properties of motor proteins to exploring collective and swarming behavior of self-organized systems.[4−8] Additionally, microtubule gliding assays are being developed for a variety of nanotechnological applications such as analyte detection, biocomputation, and mechanical sensing.[9−11] These assays have been shown to be very robust and sensitive enough to detect and analyze very small molecular fluctuations. Controlling these assays with both spatial and temporal precision has however remained a longstanding challenge. Previous studies used microfabricated or prepatterned surfaces to spatially confine, guide, and steer microtubules.[12−16] Furthermore, temporal control to activate microtubule gliding on predefined structures has been achieved through electric-field manipulation[17] and heat responsive polymer tracks,[18,19] while slow light-controlled gliding (10−20 nm/s) of actin filaments has been achieved using engineered myosin motors.[20] Additionally, control of microtubule gliding has been achieved using a light-to-heat converting layer in combination with heat-responsive polymers that compact upon heating and allow access of microtubules to surface-attached motors.[21] Furthermore, azobenzene switches fused to inhibitory peptides have been used to control kinesin-dependent motility with light.[22,23] However, the majority of these approaches requires extensive surface modifications or complicated molecular engineering, leaving simultaneous spatial and temporal control of force generation on non-predefined patterns underdeveloped.

Here we report local activation of microtubule gliding by direct light-inducible recruitment of kinesins to the surface (Figure 1). Previously, it has been shown that tunable, light-controlled interacting protein tags (TULIPs) can be efficiently used for light-induced heterodimerization to control intracellular protein recruitment and intracellular transport.[24,25] The interaction is based on the unfolding of the Jα-helix from the LOVpep core to interact with an engineered PDZ (ePDZ) domain upon blue light illumination.[24,26] We argued that light-inducible interactions based on TULIPs can be used to reversibly control local protein recruitment in vitro. Therefore,

Received: July 23, 2018
Revised: November 15, 2018
Published: November 19, 2018

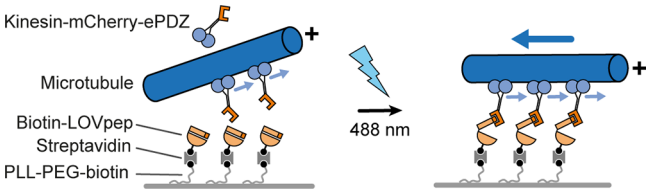

Figure 1. Schematic representation of the experimental assay for light-controlled microtubule propulsion. The LOVpep domain undergoes a conformational change upon illumination with blue light, which facilitates the binding of Kinesin-mCherry-ePDZ and induces controlled microtubule gliding.

we generated recombinant proteins fused to TULIPs to induce local heterodimerization under the control of blue light (Figure 1). We demonstrate that purified recombinant ePDZ-tagged proteins can be recruited to the coverslip with high spatiotemporal precision. Furthermore, upon recruitment of kinesin-ePDZ, microtubule gliding could be reversibly induced. This approach allows for spatiotemporal control of microtubule gliding on homogeneously coated surfaces providing an adaptive platform to manipulate microtubule motility.

First, to test whether the TULIP based interactions are sufficient for spatiotemporal control of protein recruitment in vitro, we designed an optical readout of ePDZ recruitment to the surface. We purified the LOVpep fused to biotin, which was immobilized on a microscopy coverslip functionalized with PLL−PEG−biotin and streptavidin. Subsequently, local blue light application was used to recruit purified ePDZ-mCherry from solution (Figure 2A). Indeed, when a small square region was briefly exposed to blue laser light we observed an ∼5-fold enrichment of ePDZ-mCherry in that region, compared to an ∼1.2-fold increase in a region 15 μm away from the activation light. Upon arrest of illumination, complete dissociation of ePDZ-mCherry was observed (Movie S1, Figure 2B,D). This could be efficiently repeated for multiple cycles where maximum recruitment was reached within ∼6 s and dissociation rapidly occurred with a half-life of ∼13 s in the illuminated area (Figure 2C,D). Furthermore, protein recruitment was not limited to a single shape but could be structured into a variety of patterns (Figure 2E,F). Thus, these light-induced interactions allow for sequential, reversible, and custom patterning in situ with high contrast and precision.

Next, we tested whether we could efficiently induce microtubule gliding activity by recruitment of an ePDZ domain fused to kinesin (Figure 1). After immobilization of biotin-LOVpep to the coverslip, rhodamine-labeled microtubules and kinesins were added to the reaction solution. Total internal reflection fluorescence (TIRF) imaging was then used to image the microtubules close to the surface in the absence and presence of a global 200 ms blue light pulse between each frame (Movie S2, Figure 3A,B). In the absence of blue light, microtubules displayed nondirectional movement near the coverslip with only occasional directional events. The strong microtubule enrichment near the coverslip was due to the presence of methylcellulose[27] (Figure S1), whereas the directional events were presumably due to dark-state activation or nonspecific adsorption of the motors to the surface. In contrast, upon global recruitment of kinesins to the coverslip with blue light, microtubules began to move in long directional runs along the coverslip (Figure 3A,B). Activation was reversible and induction of microtubule gliding could be repeated multiple times in the same region (Figure 3A,B). Processive microtubule gliding readily increased and decreased upon the start and stop of blue light illumination. However, complete mobilization or immobilization was observed on average after 50−100 s (Figure S1B). Determination of the fold-increase of DmKHC-mCherry-ePDZ during such illumination periods showed a gradual increase and decrease of the motor at the coverslip upon illumination or in the dark. On average a ∼ 2 fold-increase was observed and sufficient to efficiently propel microtubules (Figure S1C,D).

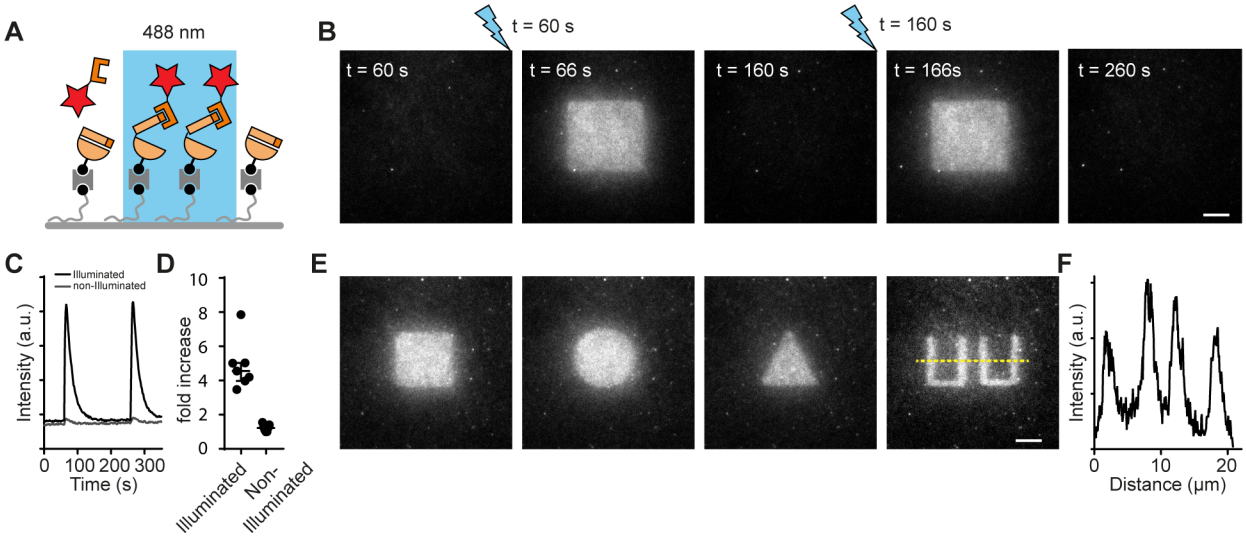

Figure 2. Spatiotemporal control of protein recruitment through light-induced heterodimerization. (A) Schematic representation of the experimental setup to recruit ePDZ-mCherry to the coverslip. (B) Locality and reversibility of ePDZ-mCherry surface binding using patterned blue light. (C) Background-corrected average intensity traces for a similar movie as shown in B. Intensities over time were measured in the illumintated square (black line) and in the nonilluminated corner of the field of view ∼20 μm apart (gray line). Single light pulses were given after 60 and 260 s. (D) Fold-increase of ePDZ-mCherry upon illumination in the illuminated center and the nonilluminated corner of the field of view of seven traces of three independent experiments. Median/IQR. (E) Repetitive ePDZ-mCherry recruitment in different patterns during the same acquisition. See also Movie S1. (F) Background corrected line scan along the yellow line indicated in D. Scale bars: 5 μm.

DOI: 10.1021/acs.nanolett.8b03011
Nano Lett. 2018, 18, 7524−7528

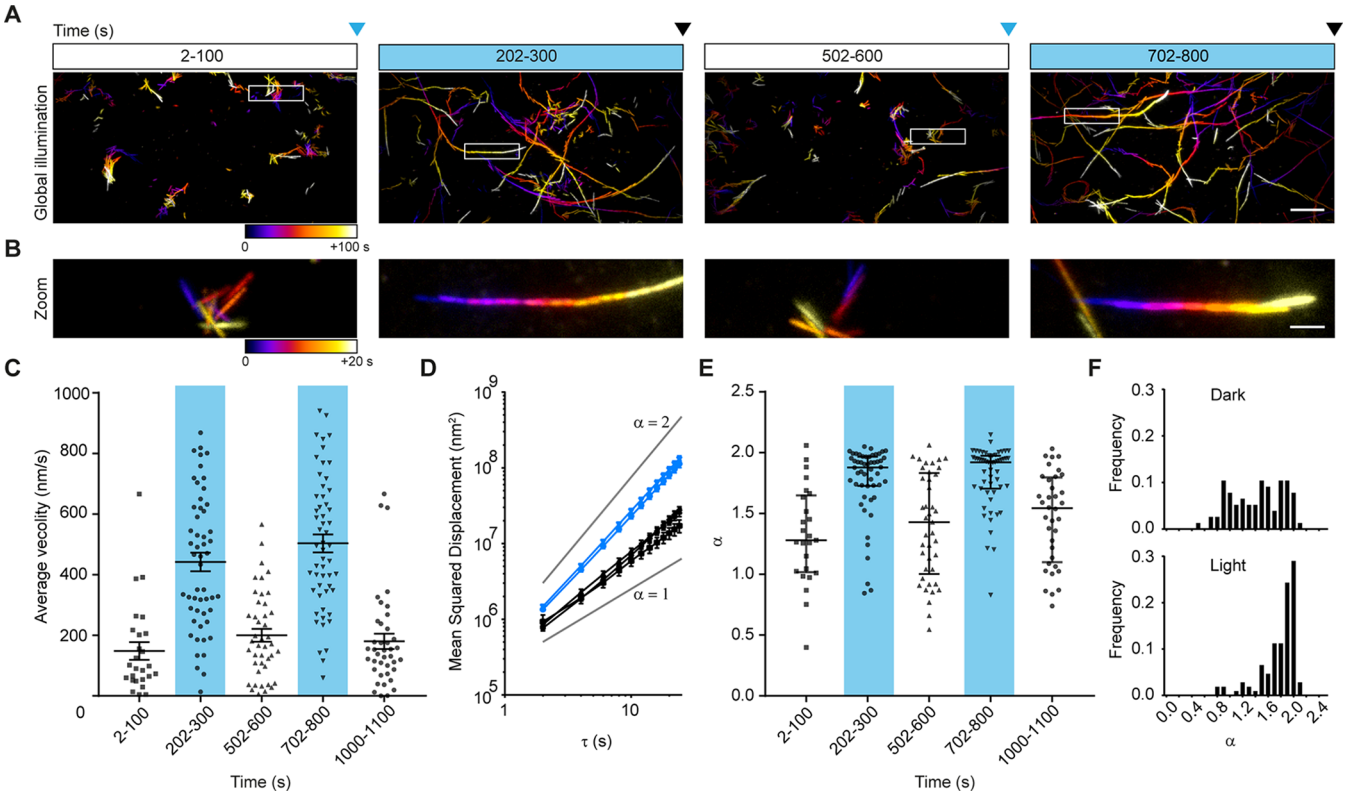

Figure 3. Global reversible control of microtubule gliding assays by blue light. (A) Temporal color-coded maximum projections of 100 one-second interval frames in the absence (white box) and presence (blue box) of light. Arrowheads indicate start (blue) and stop (black) of blue light illumination. See also Movie S2. (B) Zooms of representative 20 s tracks from the regions marked by the white boxes (A). (C) Average velocity of microtubules in (A) in the absence and presence (blue boxes) of light. Average ± s.e.m. For the five subsequent time windows of 26, 53, 43, 55, and 40 microtubule tracks were analyzed, respectively. (D) Mean-squared displacement (MSD) of microtubules in (A) in the absence (black lines) or presence (blue lines) of light. Gray lines depict lines with slopes α of 1 and 2, indicative of diffusive/nondirectional or linear/directional movement. Average ± s.e.m. (E) Fitted values of α for all individual microtubule tracks (≥16 consecutive frames) between the indicated time points. For the five subsequent time windows in the graph 25, 52, 41, 55, and 36 microtubule tracks of 3 independent experiments were analyzed, respectively. Median/IQR. (F) Frequency distribution of pooled values of α in the absence or presence of blue light. One hundred two (dark) and 107 (light) microtubule tracks of 3 independent experiments were analyzed. Scale bars: A, 10 μm; B, 2 μm.

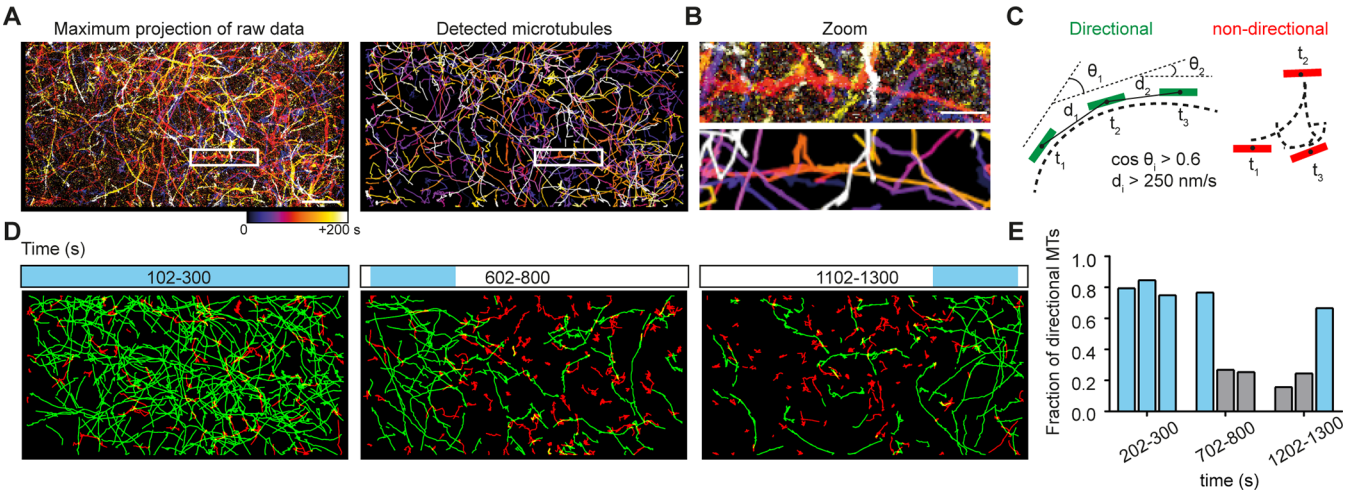

Figure 4. Local control of microtubule motility. (A) Temporal color-coded maximum projection of gliding microtubules after global activation. Raw data (left panel) and detected microtubules (right panel) over a time period of 200 s as indicated by the color-coded scale bar. See also Movie S3. (B) Zooms of the indicated regions in (A). (C) Rules for motion classification of gliding microtubules. (D) Maximum projections of classified tracks upon global and local illumination over 200 s Directional microtubule tracks are depicted in green, and nondirectional tracks in red. The blue box on top shows the illuminated area during different episodes. (E) Fraction of processive microtubules in illuminated (blue) and nonilluminated (gray) areas during each illumination episode. The three bars per indicated period indicate the directional fraction in the left, middle and right area. 234, 165, and 150 tracks were analyzed during the global, left, and right illumination episode, respectively. Scale bars: A, 20 μm; B, 5 μm.

DOI: 10.1021/acs.nanolett.8b03011
Nano Lett. 2018, 18, 7524−7528

To better understand the dynamics of the system, we traced individual microtubules for a more detailed analysis of light-activated microtubule motility. Activation of microtubule gliding led to an increase of the average velocity from ∼150 to ∼450 nm/s, which decreased again when blue light illumination was stopped (Figure 3C). Importantly, without blue light illumination the motility of most microtubules lacked an overall directionality because their frame-to-frame displacement did not have consistent direction in subsequent frames. This was revealed by an analysis of the mean-squared displacement (MSD), which reports the average squared displacement as a function of time interval. The power dependence α of the MSD with increasing time intervals τ, MSD $\propto \tau^{\alpha}$, is the anomalous diffusion exponent and indicates whether motility is completely random ($\alpha \approx 1$, diffusive), directed ($1 < \alpha \leq 2$, superdiffusive), or confined ($0 < \alpha < 1$, subdiffusive).[28] Indeed, a log−log plot of MSD(τ) averaged over all traced microtubules of the represented movie revealed that the average slope for nonilluminated microtubules (α = 1.43) increased after activation (α = 1.89) (Figure 3D). We also calculated the MSD(τ) for individual microtubules of three independent experiments and fitted the curve to MSD $\propto \tau^{\alpha}$, which revealed a significant increase in the value of α in the presence of light (Median/IQR 1.91:1.72−1.97) compared to the dark state (1.44:1.04−1.78).These results are consistent with an increase in directed microtubule displacement upon illumination (Figure 3E,F).

Finally, we tested whether our experimental setup does not only allow for temporal control but can also provide spatial control of microtubule propulsion. We used a lower magnification epifluorescence microscope equipped with a digital mirror device (DMD). In contrast to local illumination by scanning with a FRAP module, a DMD device is able to achieve fast patterned episcopic illumination, compatible with any magnification. This results in local optical control over a large field of view with low light intensities.[29] We designed an experiment where global microtubule gliding was followed by two episodes of local activation at different locations. Again efficient gliding of microtubules was observed upon global activation (Movie S3, Figure 4A, left panel). Because of the widefield illumination, signal-to-noise levels were reduced compared to the previous global gliding assays imaged in TIR F at higher magnification. Therefore, to visualize and better understand microtubule motion, we developed an automated method to detect microtubules based on cross-correlation with microtubule templates of different orientations (Figure 4A, right panel, Figure S2, Movie S4). This automated detection resulted in an accurate representation of the microtubule positions and enabled microtubule tracking (Figure 4B).

To measure the efficiency of light-induced gliding within the assay, directional and nondirectional motility were categorized into separate groups and represented by different colors, green and red, respectively (Figure 4C, Figure S2, Movie S4). Microtubule movement was classified as directional when the velocity was higher than 250 nm/s and when two consecutive velocity vectors were oriented with an angle whose cosine was larger than 0.6 (Figure 4C). The other microtubules were classified as nondirectional, which includes slow directional and diffusive, nondirectional movement. This analysis allowed us to discriminate microtubule motion under different illumination schemes where the surface was first lobally illuminated with blue light, followed by sequential illumination of the left and right area to induce local gliding (Figure 4D). During global illumination, the majority of microtubules was moving directionally across the entire field of view (75−85% directional runs). Conversely, upon local illumination confined microtubule gliding was observed in the activated areas. Quantification of the fraction of processive microtubules showed that during local activation, 77 and 67% of the microtubules were gliding directionally in the left and right area, respectively (Figure 4D,E). Furthermore, during the local illumination episodes less than 27% of microtubules were processive in the nonilluminated regions. Our results show that the use of light-inducible protein interactions provides robust spatiotemporal control of microtubule gliding assays.

Here we have developed light-inducible motor patterning on a homogeneously coated surface to directly control microtubule gliding. This approach allows for both spatial and temporal control of microtubule gliding activity within minutes on micrometer length scales with high efficiency. First, we showed that proteins fused to an ePDZ domain can be reliably coupled to surface immobilized LOVpep. Using an ePDZ-kinesin fusion, motors could be recruited to the coverslip upon activation with light to propel microtubules along the surface. Furthermore, kinesins could be locally recruited to achieve spatial control of microtubule gliding without the need for a prepatterned surface. While previous studies mostly focused on either spatial or temporal control,[12−15,17−19] our adaptive platform now offers simultaneous optical control of both, opening up new possibilities for microtubule gliding assays. Our approach is complementary to a previously developed approach in which a light-to-heat converting layer was used in combination with heat-responsive polymers that compact upon heating and allow access of microtubules to surface-attached motors.[21] However, the current approach requires less surface modifications and does not induce local temperature changes. Compared to previous developments that have used custom-engineered myosin motors to achieve slow (10−20 nm/s) light-controlled gliding of actin filaments, the use of a generic heterodimerization approach makes our approach readily applicable to a variety of different motor proteins.[20]

Our approach can be used to reconstitute and understand biological processes that rely on asymmetric forces on complex microtubule arrays. For example, light-inducible control of forces can be used to locally impose forces on reconstituted spindle-like structures or confined microtubule networks to guide the formation of complex microtubule arrays or to study cortical pulling forces.[30,31] Furthermore, light-inducible force generation could directly influence collective motion of microtubules serving as an experimental model for collective and swarming behavior. Future work could explore different light sensitive modules to improve the level of control. For example, phytochrome-based protein interactions enable red-light sensitivity[29,32] and bidirectional control, which could help to improve both temporal and spatial precision. The use of light inducible interactions to control microtubule gliding assays therefore provides exciting new possibilities for reconstituting and understanding complex biophysical and biological processes.

■ ASSOCIATED CONTENT

Supporting Information

The Supporting Information is available free of charge on the ACS Publications website at DOI: 10.1021/acs.nanolett.8b03011.

DOI: 10.1021/acs.nanolett.8b03011
Nano Lett. 2018, 18, 7524−7528

Experimental methods describing the cloning of plasmids for protein expression, protein purification, sample preparation and experimental conditions, data analysis and additional figures (PDF)

Video corresponding to Figure 2D. Sequential light-induced recruitment of ePDZ-mCherry in different patterns. Total time: 500 seconds. Acquired with 2 seconds between frames. 30 fps (AVI)

Video corresponding to Figure 3. Global reversible control of microtubule gliding assays by blue light. Total time: 1100 seconds. Acquired with 2 seconds between frames. 60 fps (AVI)

Video corresponding to Figure 4. Local control of microtubule motility. Total time: 1600 seconds. Acquired with 2 seconds between frames. 60 fps (AVI)

Video corresponding to Figure 4 and Figure S2. Conventional gliding assay with constitutively attached motors to benchmark the tracking software. Total time: 1000 seconds. Acquired with 2 seconds between frames. 60 fps (AVI)

AUTHOR INFORMATION

Corresponding Author

*E-mail: l.kapitein@uu.nl.

ORCID

Lukas C. Kapitein: 0000-0001-9418-6739

Author Contributions

[⊥]R.P.T. and C.-Y.C. contributed equally. L.C.K. conceived the research and supervised the study. R.P.T. created constructs and purified proteins with help and input from M.V. and C.Y.C. C.Y.C. performed experiments with help and input from R.P.T. R.P.T, C.Y.C., and E.A.K. analyzed data. M.K., M.D. and A.A. provided valuable suggestions and input. R.P.T., C.Y.C., and L.C.K. wrote the paper with input from all other authors.

Notes

The authors declare no competing financial interest.

ACKNOWLEDGMENTS

This work is supported by The Netherlands Organisation for Scientific Research (NWO) (NWO-ALW-VIDI 864.12.008 to L.C.K.) and the European Research Council (ERC Starting Grant 336291 to L.C.K., ERC Synergy Grant 609822 to A.A. and M.D.).

REFERENCES

(1) Nedelec, F. J.; Surrey, T.; Maggs, A. C.; Leibler, S. *Nature* **1997**, *389* (6648), 305−308.

(2) Akhmanova, A.; Steinmetz, M. O. *Nat. Rev. Mol. Cell Biol.* **2015**, *16*, 711.

(3) Kerssemakers, J. W. J.; Laura Munteanu, E.; Laan, L.; Noetzel, T. L.; Janson, M. E.; Dogterom, M. *Nature* **2006**, *442*, 709.

(4) Howard, J.; Hudspeth, A. J.; Vale, R. D. *Nature* **1989**, *342*, 154.

(5) Sumino, Y.; Nagai, K. H.; Shitaka, Y.; Tanaka, D.; Yoshikawa, K.; Chate, H.; Oiwa, K. *Nature* **2012**, *483* (7390), 448−52.

(6) Lam, A. T.; Tsitkov, S.; Zhang, Y.; Hess, H. *Nano Lett.* **2018**, *18* (2), 1530−1534.

(7) Nitzsche, B.; Bormuth, V.; Bräuer, C.; Howard, J.; Ionov, L.; Kerssemakers, J.; Korten, T.; Leduc, C.; Ruhnow, F.; Diez, S. Studying Kinesin Motors by Optical 3D-Nanometry in Gliding Motility Assays. In *Methods in Cell Biology*; Wilson, L., Correia, J. J., Eds.; Academic Press, 2010; Vol. *95*, Chapter 14; pp 247−271.

(8) Keya, J. J.; Suzuki, R.; Kabir, A. M. R.; Inoue, D.; Asanuma, H.; Sada, K.; Hess, H.; Kuzuya, A.; Kakugo, A. *Nat. Commun.* **2018**, *9* (1), 453.

(9) Chaudhuri, S.; Korten, T.; Korten, S.; Milani, G.; Lana, T.; Te Kronnie, G.; Diez, S. *Nano Lett.* **2018**, *18* (1), 117−123.

(10) Nicolau, D. V., Jr.; Lard, M.; Korten, T.; van Delft, F. C.; Persson, M.; Bengtsson, E.; Mansson, A.; Diez, S.; Linke, H.; Nicolau, D. V. *Proc. Natl. Acad. Sci. U. S. A.* **2016**, *113* (10), 2591−6.

(11) Inoue, D.; Nitta, T.; Kabir, A. M.; Sada, K.; Gong, J. P.; Konagaya, A.; Kakugo, A. *Nat. Commun.* **2016**, *7*, 12557.

(12) van den Heuvel, M. G.; Butcher, C. T.; Smeets, R. M.; Diez, S.; Dekker, C. *Nano Lett.* **2005**, *5* (6), 1117−22.

(13) Clemmens, J.; Hess, H.; Lipscomb, R.; Hanein, Y.; Bohringer, K. F.; Matzke, C. M.; Bachand, G. D.; Bunker, B. C.; Vogel, V. *Langmuir* **2003**, *19* (26), 10967−10974.

(14) Hess, H.; Matzke, C. M.; Doot, R. K.; Clemmens, J.; Bachand, G. D.; Bunker, B. C.; Vogel, V. *Nano Lett.* **2003**, *3* (12), 1651−1655.

(15) Reuther, C.; Mittasch, M.; Naganathan, S. R.; Grill, S. W.; Diez, S. *Nano Lett.* **2017**, *17* (9), 5699−5705.

(16) Bhagawati, M.; Ghosh, S.; Reichel, A.; Froehner, K.; Surrey, T.; Piehler, J. *Angew. Chem., Int. Ed.* **2009**, *48* (48), 9188−91.

(17) van den Heuvel, M. G.; de Graaff, M. P.; Dekker, C. *Science* **2006**, *312* (5775), 910−914.

(18) Ramsey, L.; Schroeder, V.; van Zalinge, H.; Berndt, M.; Korten, T.; Diez, S.; Nicolau, D. V. *Biomed. Microdevices* **2014**, *16* (3), 459−63.

(19) Schroeder, V.; Korten, T.; Linke, H.; Diez, S.; Maximov, I. *Nano Lett.* **2013**, *13* (7), 3434−8.

(20) Nakamura, M.; Chen, L.; Howes, S. C.; Schindler, T. D.; Nogales, E.; Bryant, Z. *Nat. Nanotechnol.* **2014**, *9*, 693.

(21) Reuther, C.; Tucker, R.; Ionov, L.; Diez, S. *Nano Lett.* **2014**, *14* (7), 4050−7.

(22) Rahim, M. K. A.; Fukaminato, T.; Kamei, T.; Tamaoki, N. *Langmuir* **2011**, *27* (17), 10347−10350.

(23) Kumar, K. R. S.; Kamei, T.; Fukaminato, T.; Tamaoki, N. *ACS Nano* **2014**, *8* (5), 4157−4165.

(24) Strickland, D.; Lin, Y.; Wagner, E.; Hope, C. M.; Zayner, J.; Antoniou, C.; Sosnick, T. R.; Weiss, E. L.; Glotzer, M. *Nat. Methods* **2012**, *9* (4), 379−84.

(25) van Bergeijk, P.; Adrian, M.; Hoogenraad, C. C.; Kapitein, L. C. *Nature* **2015**, *518* (7537), 111−114.

(26) Harper, S. M.; Neil, L. C.; Gardner, K. H. *Science* **2003**, *301* (5639), 1541−1544.

(27) Uyeda, T. Q. P.; Kron, S. J.; Spudich, J. A. *J. Mol. Biol.* **1990**, *214* (3), 699−710.

(28) Saxton, M. J.; Jacobson, K. *Annu. Rev. Biophys. Biomol. Struct.* **1997**, *26*, 373−99.

(29) Adrian, M.; Nijenhuis, W.; Hoogstraaten, R. I.; Willems, J.; Kapitein, L. C. *ACS Synth. Biol.* **2017**, *6* (7), 1248−1256.

(30) Heald, R.; Tournebize, R.; Blank, T.; Sandaltzopoulos, R.; Becker, P.; Hyman, A.; Karsenti, E. *Nature* **1996**, *382* (6590), 420−5.

(31) Laan, L.; Pavin, N.; Husson, J.; Romet-Lemonne, G.; van Duijn, M.; Lopez, M. P.; Vale, R. D.; Julicher, F.; Reck-Peterson, S. L.; Dogterom, M. *Cell* **2012**, *148* (3), 502−14.

(32) Levskaya, A.; Weiner, O. D.; Lim, W. A.; Voigt, C. A. *Nature* **2009**, *461* (7266), 997−1001.

DOI: 10.1021/acs.nanolett.8b03011
Nano Lett. 2018, 18, 7524−7528